Journal of Molecular Spectroscopy 254 (2009) 20–27

Contents lists available at ScienceDirect

Journal of Molecular Spectroscopy

journal homepage: www.elsevier.com/locate/jms

High sensitivity CW-cavity ring down spectroscopy of N_2O near 1.5 μm (III)

A.W. Liu [a,b], S. Kassi [a], V.I. Perevalov [c], S.M. Hu [b], A. Campargue [a,*]

[a] Laboratoire de Spectrométrie Physique (Associated with CNRS, UMR 5588), Université Joseph Fourier de Grenoble, B.P. 87, 38402 Saint-Martin-d'Hères Cedex, France
[b] Hefei National Laboratory for Physical Sciences at Microscale, University of Science and Technology of China, Hefei 230026, China
[c] Laboratory of Theoretical Spectroscopy, Institute of Atmospheric Optics, SB, Russian Academy of Sciences, 1, Akademicheckii Av., 634055 Tomsk, Russia

ARTICLE INFO

Article history:
Received 11 November 2008
Available online 24 December 2008

Keywords:
Cavity ring down spectroscopy
Nitrous oxide
N_2O
Rovibrational assignments
Effective Hamiltonian

ABSTRACT

We present the third part of the investigation of the high sensitivity absorption spectrum of nitrous oxide by CW-Cavity Ring Down Spectroscopy near 1.5 μm. In the two first contributions (A. Liu, et al., J. Mol. Spectrosc. 244 (2007) 33–47 and A. Liu, et al., J. Mol. Spectrosc. 244 (2007) 48–62) devoted to the 5905–6833 cm^{-1} region, more than 9000 line positions of five isotopologues ($^{14}N_2{}^{16}O$, $^{15}N^{14}N^{16}O$, $^{14}N^{15}N^{16}O$, $^{14}N_2{}^{17}O$ and $^{14}N_2{}^{18}O$), were rovibrationally assigned to a total of 115 bands, most of them being newly detected. The achieved sensitivity ($\alpha_{min}\sim3\times10^{-10}$ cm^{-1}) allowed for the detection of lines with intensity weaker than 2×10^{-29} cm/molecule. In this contribution, the investigated region was extended up to 7066 cm^{-1}. The analysis based on the predictions of the effective Hamiltonian model has allowed assigning about 1500 transitions to 17, 1, 2 and 1 bands of the $^{14}N_2{}^{16}O$, $^{14}N^{15}N^{16}O$, $^{15}N^{14}N^{16}O$ and $^{14}N_2{}^{18}O$ isotopologues, respectively. Eleven of these 21 bands are newly reported, while the observations of the transitions are extended to higher J values for most of the others. The band by band analysis has allowed reproducing the measured line positions within the experimental uncertainty (about 1×10^{-3} cm^{-1}) and determining the corresponding spectroscopic parameters. A detailed analysis of the rovibrational perturbations affecting three bands of $^{14}N_2{}^{16}O$ is presented.

1. Introduction

This work is a continuation of our previous studies of the absorption spectrum of nitrous oxide by high sensitivity CW-Cavity Ring Down Spectroscopy (CW-CRDS) [1,2] near 1.5 μm. We have developed a fibered CW-CRDS spectrometer using Distributed Feed-Back (DFB) diode lasers dedicated to the characterization of this important atmospheric window of transparency. 40 DFB diode lasers were purchased in order to cover continuously the 5905–6833 cm^{-1} region. Thanks to the high sensitivity achieved (noise equivalent absorption $\alpha_{min}\sim3\times10^{-10}$ cm^{-1}), more than 9000 transitions belonging to a total of 115 bands of five isotopologues were rovibrationally assigned on the basis of the predictions of the global effective Hamiltonian models [3–6].

In this third contribution, the recordings were extended up to 7066 cm^{-1} thanks to nine additional DFB lasers. About 1500 transitions due to 17, 1, 2 and 1 bands for the $^{14}N_2{}^{16}O$, $^{14}N^{15}N^{16}O$, $^{15}N^{14}N^{16}O$ and $^{14}N_2{}^{18}O$ isotopologues, respectively, were identified in these new spectra. Note that the HITRAN [7] notation will be used along the paper, for the four isotopologues contributing to the spectrum: $^{14}N_2{}^{16}O$: 446, $^{14}N^{15}N^{16}O$: 456, $^{15}N^{14}N^{16}O$: 546 and $^{14}N_2{}^{18}O$: 448. Eleven of these 21 bands are newly reported, while the observation of additional transitions of previously analyzed bands has yielded a refined determination of their spectroscopic parameters. The band by band rovibrational assignment and fit are presented in Section 3 which also includes the detailed analysis of the rovibrational perturbations affecting three bands of $^{14}N_2{}^{16}O$.

2. Experiment

The reader is referred to Refs. [1,8–11] for the description of our fibered DFB diode laser CW-CRDS spectrometer. The 6828–7066 cm^{-1} region was covered with the help of nine newly purchased fibered DFB diode lasers, each of them having a typical tuning range of 30 cm^{-1}. About 70 min are needed for a complete temperature scan from −10 to 65 °C. The considered spectral region is approaching the upper energy limit of the high reflectivity region of the used mirror set. In consequence, the typical ringdown time decreases from 60 μs at 6400 cm^{-1} to 36 μs at 7050 cm^{-1}. Consequently, the noise equivalent absorption coefficient increases from $\alpha_{min}\sim2\times10^{-10}$ cm^{-1} near 6400 cm^{-1} up to $\alpha_{min}\sim1\times10^{-9}$ cm^{-1} near 7050 cm^{-1}. Fig. 1 illustrates the 4 to 5 decades dynamic range on the intensity scale achieved with our set up: absorption coefficient ranging from $\alpha_{min}\sim10^{-5}$ cm^{-1} down to the noise level at 3×10^{-10} cm^{-1} can be measured from a single spectrum.

Each 30 cm^{-1} wide spectrum recorded with one DFB laser was calibrated independently on the basis of the wavelength values

* Corresponding author. Fax: +33 4 76 63 54 95.
E-mail address: Alain.Campargue@ujf-grenoble.fr (A. Campargue).

0022-2852/$ - see front matter © 2008 Elsevier Inc. All rights reserved.
doi:10.1016/j.jms.2008.12.006

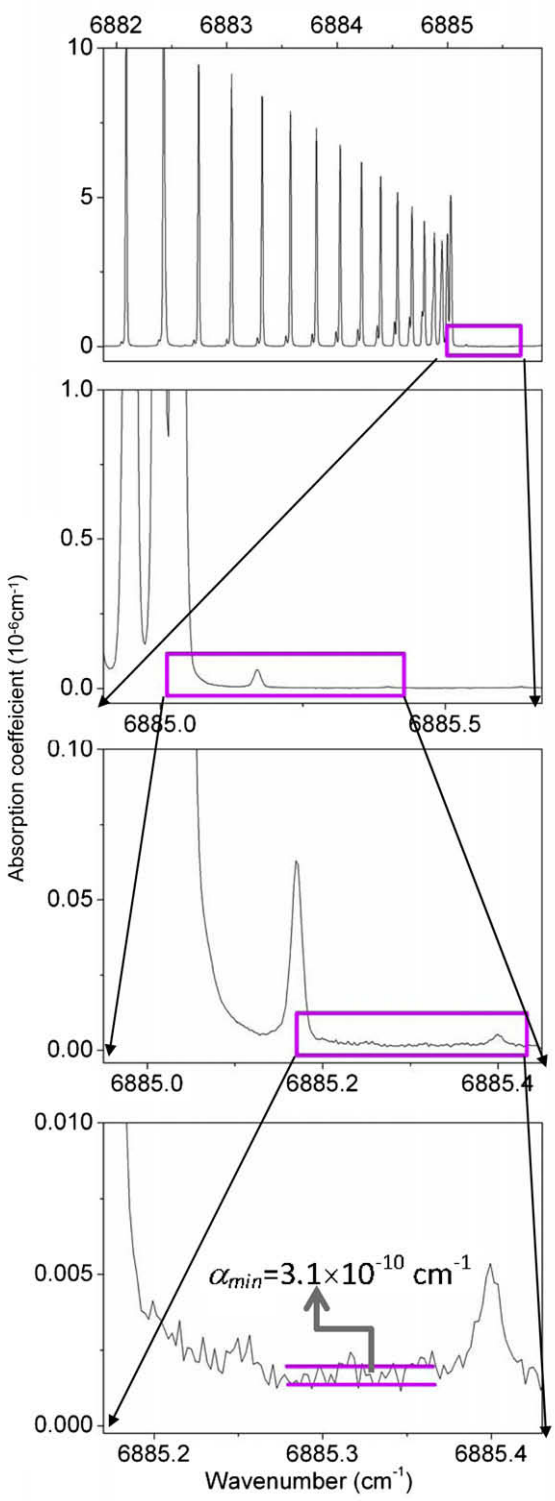

Fig. 1. CW-CRDS spectrum of natural nitrous oxide near 6855 cm^{-1} showing the band head of the 2002e–0000e centered at 6868.55 cm^{-1}. The sample pressure was 40.0 Torr. Four successive enlargements of the CW-CRDS spectrum illustrates the high dynamics achieved by the CW-CRDS spectrometer allowing for the measurement of absorption coefficient differing by four orders of magnitude (from 10^{-5} cm^{-1} to the noise level at about 3.1×10^{-10} cm^{-1}).

provided by the Michelson-type wavemeter (Burleigh WA-1650, 60 MHz resolution and 100 MHz accuracy at this wavelength). The calibration was further refined by stretching the whole spectrum in order to match accurate positions of reference lines. The studied region corresponds to a strong absorption region of H_2O and many H_2O transitions are observed in our spectra. Their line positions as provided by the HITRAN database were used for calibration. The typical uncertainty on the line positions is 1×10^{-3} cm^{-1} as confirmed by the typical values of the (obs.−calc.) *rms* deviations obtained in the fit of the spectroscopic parameters (see below).

The spectra were recorded at different pressures ranging from 10 to 40 Torr. The observed line profile is then mostly a Gaussian function fixed by the Doppler broadening (FWHM $\sim$ 11×10^{-3} cm^{-1} at 296 K).

3. Rovibrational analysis

The N_2O vibrational pattern has a polyad structure resulting from the approximate relations $\omega_3 \approx 2\omega_1 \approx 4\omega_2$ between the harmonic frequencies. The observed transitions were assigned on the basis of the predictions of the effective rovibrational Hamiltonian [3–6] which is a polyad model. The mixing between the $V_1 l_2 V_2 V_3$ states being important for many levels in our region, the vibrational states are preferably labeled using the triplet $\{P = 2V_1 + V_2 + 4V_3,\ l_2,\ i\}$ where the index i increases with the energy.

In the studied region, all but one band correspond to a $\Delta P = 12$ variation of the polyad quantum number, the Σ–Π hot band of $^{14}N_2{}^{16}O$ at 7076.508 cm^{-1} corresponding to $\Delta P = 13$. The vibrational assignments and fractions respective to the normal mode basis states are listed in Table 1 for the bands of $^{14}N_2{}^{16}O$, $^{14}N^{15}N^{16}O$, $^{15}N^{14}N^{16}O$ and $^{14}N_2{}^{18}O$ analyzed in the 6833–7066 cm^{-1} region. The strongest band at 6868.55 cm^{-1} corresponds to the excitation of the (1206) state – (2002) in normal mode notation. It is the only band included in the HITRAN database [7] in our region (see Fig. 2). The Σ–Σ band reaching the (12010) state has a comparable band strength but it is centered at 7137.1270 cm^{-1} in the case of $^{14}N_2{}^{16}O$ *i.e.* above the upper limit of our energy region. Then only high J values in the P branch could be observed for this band. Thanks to the isotopic shift to lower energies, the whole rotational structure of this band could be observed in the case of the 456, 546 and 448 isotopologues. It is interesting to note that the isotopic substitution leads to important changes in the expansion of the (12010) state in the normal mode basis (Table 1). The sensitivity of the interaction scheme to isotopic substitution is such that the dominant vibrational normal state is (24^01) in the case of 546 but (40^01) for the other three isotopologues.

The standard expression of the vibration–rotation energy levels was used for the fit of the spectroscopic parameters:

$$F_v(J) = G_v + B_v J(J+1) - D_v J^2(J+1)^2 + H_v J^3(J+1)^3, \quad (1)$$

where G_v is the vibrational term value, B_v is the rotational constant, D_v and H_v are centrifugal distortion constants. The spectroscopic parameters were fitted directly to the observed wavenumbers, the lower state rotational constants (given in Refs. [1,2]) being constrained to their literature values [12].

3.1. The $^{14}N_2{}^{16}O$ isotopologue

The seventeen bands of the $^{14}N_2{}^{16}O$ isotopologue which were analyzed are presented in Fig. 2 which includes the overview comparison with the HITRAN database [7]. HITRAN2004 database is based on the SISAM.N2O line list established by Toth [12]. In the 6833–7066 cm^{-1} region, it provides 58 lines for nitrous oxide while we could assign 1324 transitions. Eight of the reported bands are newly observed. In the case of the four bands centered below 6860 cm^{-1}, only P lines could be observed in our previous CW-

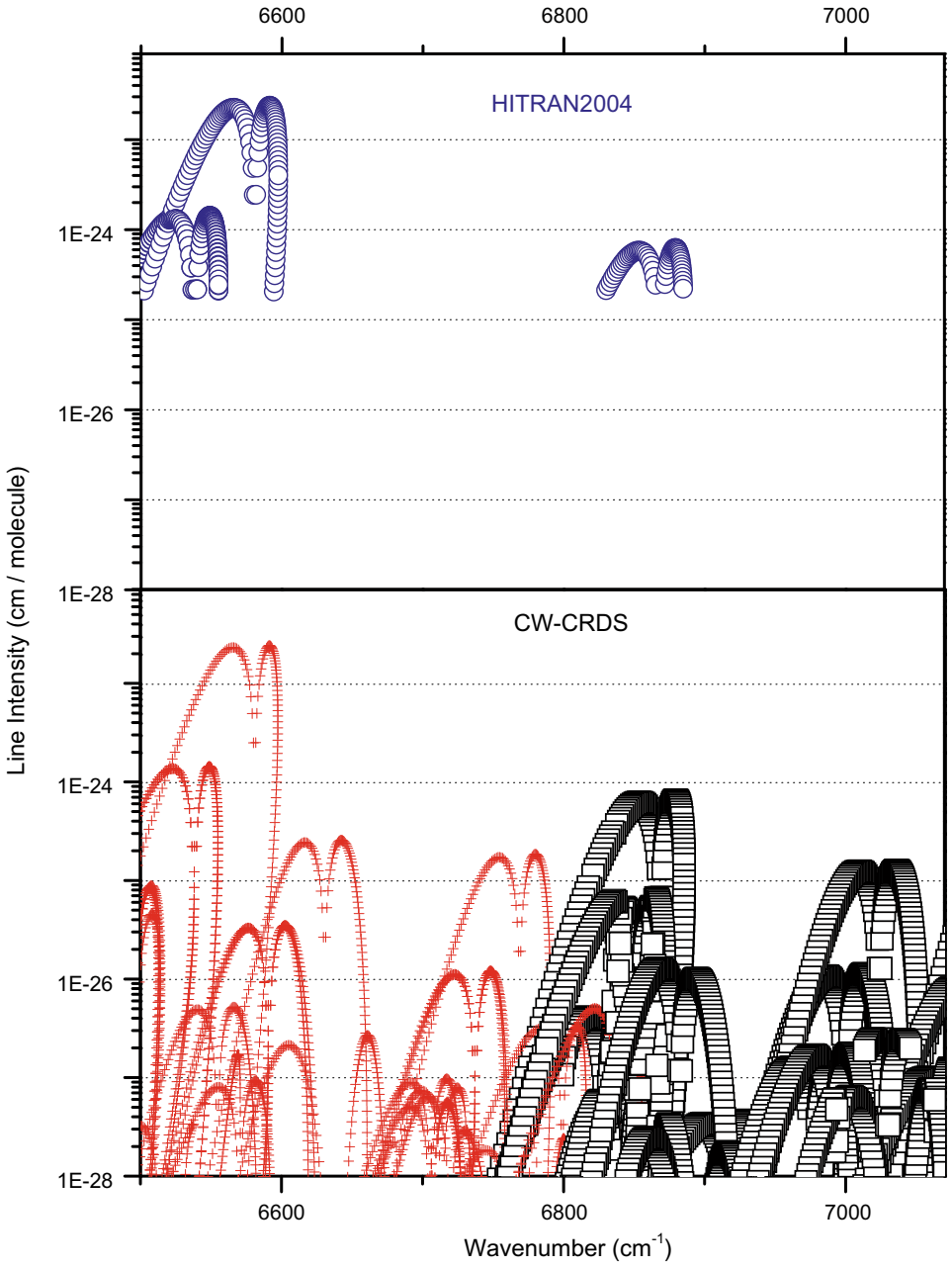

Fig. 2. Overview of the spectrum of the main isotopologue, $^{14}N_2{}^{16}O$, of nitrous oxide between 5905 and 7066 cm^{-1}. Note the logarithmic scale adopted for the line intensities. *Upper panel:* HITRAN database [7]. *Lower panel:* Bands observed by CW-CRDS as predicted by the polyad model of effective Hamiltonian [4,16]. The crosses correspond to the bands previously reported in Refs. [1,2] while the open squares correspond to the present work.

CRDS spectra below 6833 cm^{-1} [1,2]. The present recordings allow observing their *R* branches. This is interesting as three of these bands are affected by perturbations (see below).

The spectroscopic parameters retrieved from the fit of the line positions are listed in Table 2. The *rms* values of the (obs.−calc.) deviations are generally on the order of 1.5×10^{-3} cm^{-1} which is consistent with the uncertainty on the line positions. The observed and calculated line positions are provided as Supplementary material attached to this paper.

We have reviewed and included in Table 2, the band parameters previously reported in the literature. The previous investigations were performed by Fourier Transform Spectroscopy by Toth (absorption path length up to 422 meters [12]), Weirauch et al. [13] (up to 48.2 m path length) and Wang et al. [14] (105 m path length). Our CW-CRDS spectra allowed increasing to higher *J* values the transitions observed in the rotational structure of the previously reported bands. Note that a few of the upper levels presently detected, were previously observed as upper states of other bands lying in different spectral regions. The corresponding bands and reference have been indicated in the last column of Table 2, excluding the CW-CRDS results of Refs. [1,2].

As discussed in Refs [1,2], the 3002–0200 band at 6830.45 cm^{-1} and the 0911–0110 and 2112–0110 bands at 6852.63 and 6854.16 cm^{-1} respectively, are perturbed by intrapolyad anharmonic resonance interaction (The matrix elements of the respective resonance interaction operators are given in Ref. [2]). As only part of the respective *P* branches could be observed in the recordings of Refs. [1,2], only a partial analysis was possible at that time. The complete spectral coverage of these bands allows a deeper investigation of these perturbations.

Table 1
Vibrational assignment and corresponding fractions respective to the basis states for the bands of $^{14}N_2{}^{16}O$, $^{14}N^{15}N^{16}O$, $^{15}N^{14}N^{16}O$ and $^{14}N_2{}^{18}O$ analyzed in the CW-CRDS spectra between 6800 and 7066 cm^{-1}.

ΔP	Band[a]	(Pl_2i)[b]	ΔG_v (cm^{-1})	Basis states[c]	%Fraction[d]
446 cold bands					
12	2002e–0000e	(1206)	6868.5501	$(20^02)/(1202)$	71/21
12	0801e–0000e	(1207)	6882.6922	$(08^01)/(24^01)/(32^01)$	40/34/22
12	0821e–0000e	(12212)	6891.7531	$(08^21)/(24^21)/(32^21)$	41/39/18
12	3201e–0000e	(1208)	7024.0937	$(32^01)/(16^01)/(08^01)$	37/23/22
12	0(12)00e–0000e	(1209)	7029.8422	$(012^00)/(36^00)/(44^00)/(110^00)$	27/27/21/17
12	3221e–0000e	(12215)	7036.9676	$(32^21)/(16^21)/(08^21)$	30/18/16
12	4001e–0000e	(12010)	7137.1270	$(40^01)/(24^01)/(16^01)$	46/21/21
446 hot bands					
12	3002e–0200e	(1408)	6830.4520	$(30^02)/(14^02)$	35/33
12	2222e–0220e	(14215)	6837.7374	$(22^22)/(14^22)$	49/37
12	0911e–0110e	(1316)	6852.6332	$(09^11)/(33^11)/(25^11)$	37/30/24
12	2112e–0110e	(1317)	6854.1609	$(21^12)/(13^12)$	57/31
12	3002e–0200e	(1409)	6915.8210	$(30^02)/(22^02)$	50/29
12	4201e–0200e	(14010)	6977.4184	$(42^01)/(010^01)$	28/28
12	5001e–1000e	(14012)	6991.4216	$(50^01)/(18^01)/(42^01)$	23/22/21
12	0911e–0110e	(1318)	7000.6451	$(09^11)/(33^11)/(41^11)$	25/24/20
12	5001e–1000e	(14014)	7091.4454	$(50^01)/(26^01)$	48/17
13	0203e–0110e	(1401)	7076.5084	(02^03)	88
456 cold bands					
12	2401e–0000e	(12010)	7051.7752	$(24^01)/(40^01)/(32^01)$	34/30/18
546 cold bands					
12	3201e–0000e	(1208)	6957.8995	$(32^01)/(08^01)/(16^01)/(40^01)$	37/23/21/16
12	4001e–0000e	(12010)	7065.5255	$(40^01)/(16^01)/(24^01)$	53/22/17
448 cold bands					
12	4001e–0000e	(12010)	7006.3390	$(40^01)/(24^01)$	60/26

[a] $V_1V_2l_2V_3$. According to the maximum value of the modulo of the expansion coefficients of the eigenfunction as obtained from the effective Hamiltonian model [4].
[b] Cluster labeling notation: $(P = 2V_1 + V_2 + 4V_3, l_2, i)$ for the upper state of the band; i is the order number within the cluster increasing with the energy.
[c] Only basis states with modulo of expansion coefficients larger than 0.4 are presented.

The (1408) upper state (3002 in normal modes notation) of the first band is perturbed by the (1407) dark state (3401 in normal modes notation). The two other bands have upper states, namely (1316) and (1317), which are in strong interaction around the energy levels crossing at $J = 17$. Fig. 3 shows the deviation from their respective unperturbed positions as calculated from the respective spectroscopic parameters of Table 2. The resulting energy crossings are illustrated on the reduced energy plots of Fig. 4 which represent the difference between the experimental energy levels and the unperturbed energy levels of the (1316) state obtained by using the spectroscopic parameters listed in Table 2. In the fit of the spectroscopic parameters (Table 2), only J values above the energy crossing were used as input data. It leads to effective values which should be used with caution. In particular, Fig. 3 shows that the energy levels of the (1317) state calculated with these parameter values, deviate by about 0.08 cm^{-1} for the low J transitions. In order to provide a more accurate value of the band centre, we have performed a separate fit of the band centre and main rotational constant by using only low J values transitions. The corresponding values are included in Table 2.

Finally, the Π–Π band at 7000.645 cm^{-1} was also found perturbed. While transitions with J values up to 60 were assigned only those with J less than 20 could be reproduced using the single band polynomial expansion Eq. (1). The (1318) upper level (0911 in normal mode notation) of this band is affected by a strong Fermi interaction ($\omega_3 \approx 2\omega_1$) with the (1319) level (4510 in normal mode notation). These two levels are very close (the energy separation is predicted to be about 3 cm^{-1}) but there is no crossing for any J values. We draw the attention of the readers to the fact that the (1316) and (1318) vibrational states have the same 0911 labeling in the normal mode notations.

3.2. The 456, 546 and 448 minor isotopologues

As mentioned above, the bands reaching the (12010) upper state could be detected for these three minor isotopologues which are in natural abundance in our sample (3.64×10^{-3} abundance for 456 and 546; 1.98×10^{-3} for 448 [7]). In addition, we could identify the 3201e–0000e band of the 546 isotopologue at 6957.90 cm^{-1}. These observations are the highest energy bands reported so far for the 546 and 448 isotopologues. In the case of the 456 species, FTS spectra have been recently obtained by Fourier Transform Spectroscopy in Hefei by using a sample with a 97.4% isotopic enrichment and absorption path lengths up to 105 m [15]. 107 bands could be detected and analysed between 4000 and 9000 cm^{-1}. The retrieved line positions were used as input data for a global fit of the effective Hamiltonian parameters [15]. The spectroscopic parameters relative to the minor isotopologues are presented in Table 3. The $^{14}N^{15}N^{16}O$ parameters values obtained by Ni et al. [15] from a larger input data set are included in this Table for comparison.

4. Discussion and conclusion

The difference between the line positions of the 446 isotopologue measured in the CW-CRDS spectrum between 6800 and 7066 cm^{-1} and their values predicted by the effective rovibrational Hamiltonian [4] are plotted in Fig. 5. The predictive ability of the effective Hamiltonian model is good for this main isotopologue since the majority of the residuals lies between −0.04 and 0.04 cm^{-1}. In particular, the predictions proved to be fully satisfactory to quantitatively account for the observed perturbations. However, compared to our previous CW-CRDS results [1,2], it seems that the deviations tend to increase with the energy, a number of values being on the order of ± 0.07 cm^{-1}.

Table 2
Spectroscopic parameters (in cm^{-1}) of the rovibrational bands of $^{14}N_2{}^{16}O$ assigned for the CW-CRDS spectra between 5906 and 6833 cm^{-1}. The cold and hot bands are listed successively and ordered according to their ΔG_v values. The lower state constants were taken from Ref. [12] and are reproduced in Refs. [1,2].

ΔG_v[a]	Type	$V_1V_2l_2V_3$[b]	(Pl_2i)	G_v	B_v	$D_v \times 10^7$	$H_v \times 10^{12}$	*observed lines*	*n/N*[c]	*rms* $\times 10^3$	Previous reports[d]
6830.45203(57)	Σ–Σ perturbed[f]	3002e–0200e	(1408)	7998.58433(57)	0.4095520(68)	0.46(16)	[2.955393]	P49/R39	30/64	1.4	*3002e–0000e*^{We}
6837.73740(42)	Δ–Δ	2222e–0220e	(14215)	8015.48207(42)	0.4103177(27)	1.501(38)	15.8(15)	P38/R42	62/65	1.4	
6837.73653(59)		2222e–0220f		8015.48120(59)	0.410347(22)	3.6(13)	[0.095]	Q12	8/8	0.8	
6837.73883(36)		2222f–0220f		8015.48350(36)	0.4102954(25)	1.599(48)	5.7[22]	P41/R39	59/65	1.2	
6852.6332(40)	Π–Π perturbed[f]	0911e–0110e	(1316)	7441.4011(40)	0.4147763(79)	2.584(36)	[-0.01714]	P39/R38	22/47	1.2	
6852.6290(53)		0911f–0110f		7441.3969(53)	0.417648(16)	2.36(15)	-28.6(45)	P44/R37	27/50	1.3	
6854.1609(20)	Π–Π perturbed[f,g]	2112e–0110e	(1317)	7442.9287(20)	0.4090450(31)	1.758(15)	1.77(21)	P64/R57	54/109	1.0	*2112e–0110e*^{We}
				7443.00089(65)[g]	*0.4092237(83)*[g]						
6854.1649(22)		2112f–0110f		7442.9328(22)	0.4100606(40)	1.729(22)	3.33(36)	P61/R40	43/96	1.2	
				7443.00506(49)[g]	*0.410185(10)*[g]						
6868.55007(16)	Σ–Σ	2002e–0000e	(1206)	6868.55007(16)	0.40862574(43)	1.6089(27)	0.712(44)	P67/R59	119/122	0.8	*2002e–1000e*^{Wa}
		2002e–0000e^{T}		*6868.54982(50)*	*0.40862919(96)*	*1.698(19)*	*5.89(85)*				
		2002e–0000e^{We}		*6868.55062(28)*	*0.4086257(14)*	*1.631(16)*	*1.76(48)*		*96/97*	*1.2*	
		2002e–0000e^{L}		*6868.550165(89)*	*0.4086249(1)*	*1.60282(38)*	*0.608(62)*	*P67/R35*	*99/99*	*0.5*	
6882.69219(23)	Σ–Σ	0801e–0000e	(1207)	6882.69219(23)	0.41604441(96)	5.8166(93)	31.60(25)	P51/R52	88/96	0.9	
		0801e–0000e^{Wa}		*6882.7117(16)*	*0.4159792(49)*	*4.985(28)*		*R40*	*25/34*	*3.2*	
6891.7531(21)	Δ–Σ	0821e–0000e	(12212)	6891.7531(21)	0.4163320(45)	-0.161(22)	[-0.016529]	P40/R40	27/33	1.3	
6915.82102(36)	Σ–Σ	3002e–0200e	(1409)	8083.95332(36)	0.4071832(18)	1.314(17)	[2.955393]	P29/R32	46/51	1.1	*3002e–0000e*^{We}
6977.41838(85)	Σ–Σ	4201e–0200e	(14010)	8145.55068(85)	0.4146268(69)	10.33(13)	185.4(69)	P38/R34	48/56	2.1	*4201e–0000e*^{We} *4201e–0000e*^{Wa}
6991.42161(49)	Σ–Σ	5001e–1000e	(14012)	8276.32495(49)	0.4115886(30)	3.380(43)	10.2(16)	P44/R31	60/63	1.5	
7000.64514(32)	Π–Π Perturbed[f]	0911e–0110e	(1318)	7589.41301(32)	0.4131889(84)	7.48(54)	146(97)	P60/R49	30/97	0.5	
7000.64540(54)		0911f–0110f		7589.41327(54)	0.4156904(96)	9.54(32)	[-0.01766]	P59/R52	31/93	1.3	
		0911–0110^{Wa}						*P32/R28*	*48/77*	*3.15*	
7024.09370(34)	Σ–Σ	3201e–0000e	(1208)	7024.09370(34)	0.41362463(98)	3.7214(65)	11.77(11)	P67/R63	118/127	1.5	
		3201e–0000e^{We}		*7024.09258(38)*	*0.4136385(19)*	*3.909(23)*	*17.89(73)*		*87/93*	*1.5*	
7029.84224(54)	Σ–Σ	0(12)000e–0000e	(1209)	7029.84224(54)	0.4198878(46)	12.753(95)	155.4(53)	P36/R30	38/40	1.2	
7036.9676(95)	Δ–Σ	3221e–0000e[h]	(12215)	7036.9676(95)	0.414992(35)	8.53(37)	219(12)	P40	18/22	1.7	
7076.5085(14)	Σ–Π	0203e–0110e[h]	(1401)	7665.2764(14)	0.4097734(44)	2.386(29)	[-0.01714]	P38	13/14	1.2	*0203e–0000e*^{We} *0203e–0000e*^{O} *0203e–0200e*^{T}
7091.4454(60)	Σ–Σ	5001e–1000e[h]	(14014)	8376.3488(60)	0.408931(12)	2.026(56)	[0.146666]	P40	11/12	1.3	*5001e–0000e*^{We}
7137.126973(74)	Σ–Σ	4001e–0000e[e]	(12010)	7137.126973(74)	0.41096972(22)	2.3455(14)	2.541(23)	P56/R35	76/76	0.3	
		4001e–0000e^{We}		*7137.12818(21)*	*0.41096866(91)*	*2.3353(89)*	*23.0(24)*		*98/100*	*0.9*	
		3201e–0000e^{T}		*7137.12706(29)*	*0.41096848(32)*	*2.3071(19)*					

Notes: The lower state constants and those appearing between square brackets were held fixed at the values of Ref. [12]. The uncertainties are given in parenthesis in the unit of the last quoted digit. Except for our previous observations [1,2], when a given band has been previously analyzed, the corresponding spectroscopic parameters are given in italics for comparison: ^{T}Toth [12], ^{Wa}Wang et al. [14], ^{We}Weirauch et al. [13], ^{O}Oshika et al. [17].

[a] Difference between the upper and lower vibrational term values.

[b] Normal mode labeling according to the maximum value of the modulo of the expansion coefficients of an eigenfunction.

[c] *n*: number of transitions included in the fit; *N*: number of assigned rotational transitions.

[d] Previous observations of the upper level through a different band.

[e] For this band, the set of the CRDS line positions used for the fit of the rovibrational parameters was completed by line positions provided by the HITRAN database [7] (as indicated in the Supplementary material).

[f] Bands perturbed by intrapolyad anharmonic interaction (see Text). The fitted values of the parameters should be considered with caution as only part of the rotational levels was used as input data of the fit.

[g] G_v and B_v values were obtained by fitting the transition wavenumbers corresponding to low *J* values in order to determine a more accurate value of the centre of this perturbed band (see Text and Fig. 3).

[h] The fitted values of the parameters of these bands should be considered with caution as only part of the rotational levels of the *P* branch was used as input data of the fit.

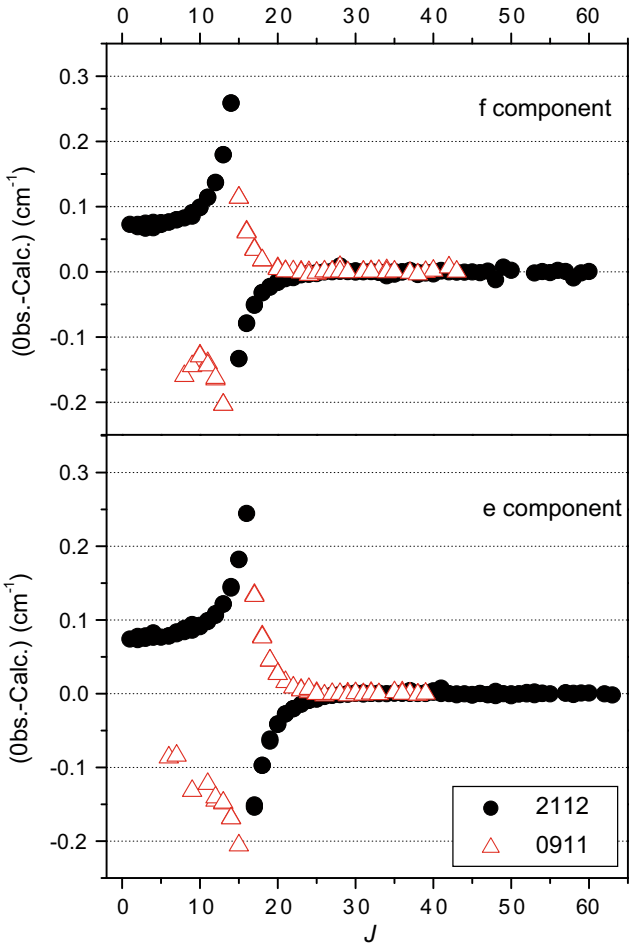

Fig. 3. Difference between the observed energy levels of the (1316) and (1317) interacting states of $^{14}N_2{}^{16}O$, with the (unperturbed) values calculated with the spectroscopic parameters of Table 2. The upper and lower panels are relative to the *e* and *f* sub bands of the Π–Π hot band from the (111) lower state. For each J_{up} value, the values of the energy level obtained from the $R(J_{up}-1)$ and $P(J_{up}+1)$ transitions are plotted. The open triangles and full circles correspond to levels with a dominant character of the (1316) and (1317) states, respectively. Note that the effective parameters used for the calculated energy levels were obtained by using wavenumber corresponding to transitions with high *J* values (see Text for details).

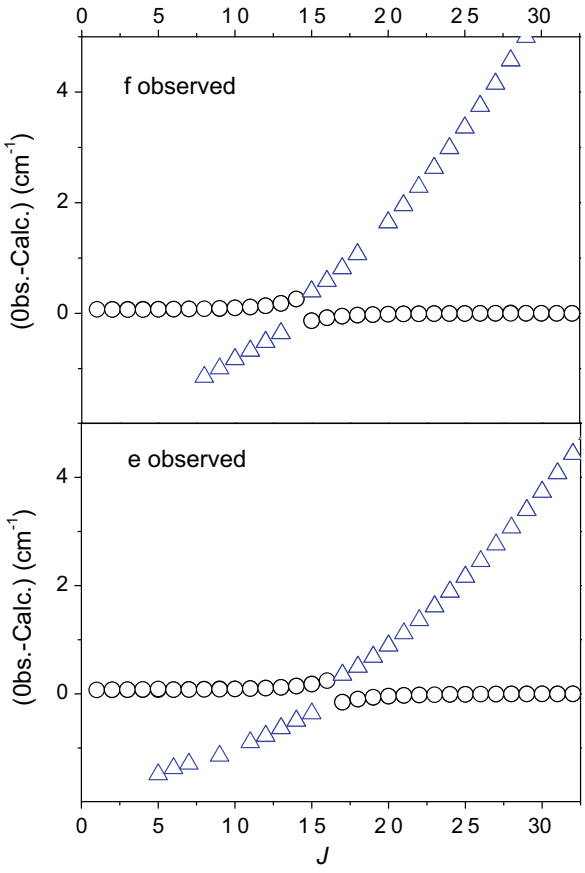

Fig. 4. Reduced energy plot for the (1316) and (1317) interacting states. For the *e* and *f* components of these two states, the difference between the experimental energy levels and the unperturbed energy levels of the (1316) state are plotted. The unperturbed energy levels of the (1316) state were obtained by using the spectroscopic parameters listed in Table 2. The upper and lower panels are relative to the *f* and *e* sub bands of the (1316)–(111) Π–Π hot band at 6852.63 cm^{-1}, respectively. For each J_{up} value, the values of the energy level obtained from the $R(J_{up}-1)$ and $P(J_{up}+1)$ transitions are plotted. The open triangles and circles correspond to levels with a dominant character of the (1317) and (1316) state, respectively.

The high sensitivity and the high dynamics of our CW-CRDS spectrometer have allowed observing 21 bands, 11 of them being newly reported, while the observations of the transitions were extended to higher *J* values for most of the others. The 1324 transitions which have been presently rovibrationally assigned together with the transitions reported in our preceding reports [1,2], lead to a set of about 10,500 transitions belonging to a total of 132 bands of five isotopologues of nitrous oxide identified in the whole 5905–7066 cm^{-1} spectral region. Compared to the HITRAN database which provides 841 transitions in the same region, all due to the main 446 isotopologue, the improvement is particularly significative allowing for a much better knowledge of the spectroscopy of nitrous oxide in the 1.5 μm atmospheric window.

The density of the N_2O lines measured in our spectrum is about 10 lines/cm^{-1}. This spectral congestion made the assignment process very laborious, in particular in the present spectral region

Table 3
Spectroscopic parameters (in cm^{-1}) of $^{14}N^{15}N^{16}O$, $^{15}N^{14}N^{16}O$ and $^{14}N_2{}^{18}O$ rovibrational bands analyzed in the CW-CRDS spectrum of nitrous oxide between 6800 and 7066 cm^{-1}.

	G_v	Type	$V_1V_2l_2V_3$[a]	(Pl_2i)	B_v	$D_v \times 10^7$	$H_v \times 10^{12}$	observed lines	n/N[b]	$rms \times 10^3$
$^{14}N^{15}N^{16}O$	7051.77518(87)	Σ–Σ	1601e–0000e	(12 0 10)	0.4111447(86)	2.60(18)		P22/R19	24/26	1.2
	7051.77452(94)	*Σ–Σ*	*1601e–0000e*^{Ni}	*(12 0 10)*	*0.4114508(47)*	*2.5633(55)*	*3.71(17)*	*P49/R47*	*92/95*	*0.39*
$^{15}N^{14}N^{16}O$	6957.89949(37)	Σ–Σ	3201e–0000e	(12 0 8)	0.3996436(24)	3.058(36)	6.2(15)	P43/R37	63/67	1.2
	7065.52553(36)	Σ–Σ	4001e–0000e	(12 0 10)	0.3971445(23)	2.092(31)	2.6(11)	P45	35/37	1.0
$^{14}N_2{}^{18}O$	7006.33901(45)	Σ–Σ	4001e–0000e	(12 0 10)	0.3878391(37)	1.822(68)	13.1(34)	P36/R36	51/53	1.3

Notes: The ground state constants were held fixed at the values of Ref. [12]. The uncertainties are given in parenthesis in the unit of the last quoted digit. The 1601e–0000e band of $^{14}N^{15}N^{16}O$ has been previously analyzed from FTS spectrum obtained with 97.4% enrichment in $^{14}N^{15}N^{16}O$. The corresponding spectroscopic parameters are given in italics for comparison: ^{Ni}Ni et al. [15].

[a] Normal mode labeling according to the maximum value of the modulo of the expansion coefficients of an eigenfunction.

[b] *n*: number of transitions included in the fit; *N*: number of assigned rotational transitions.

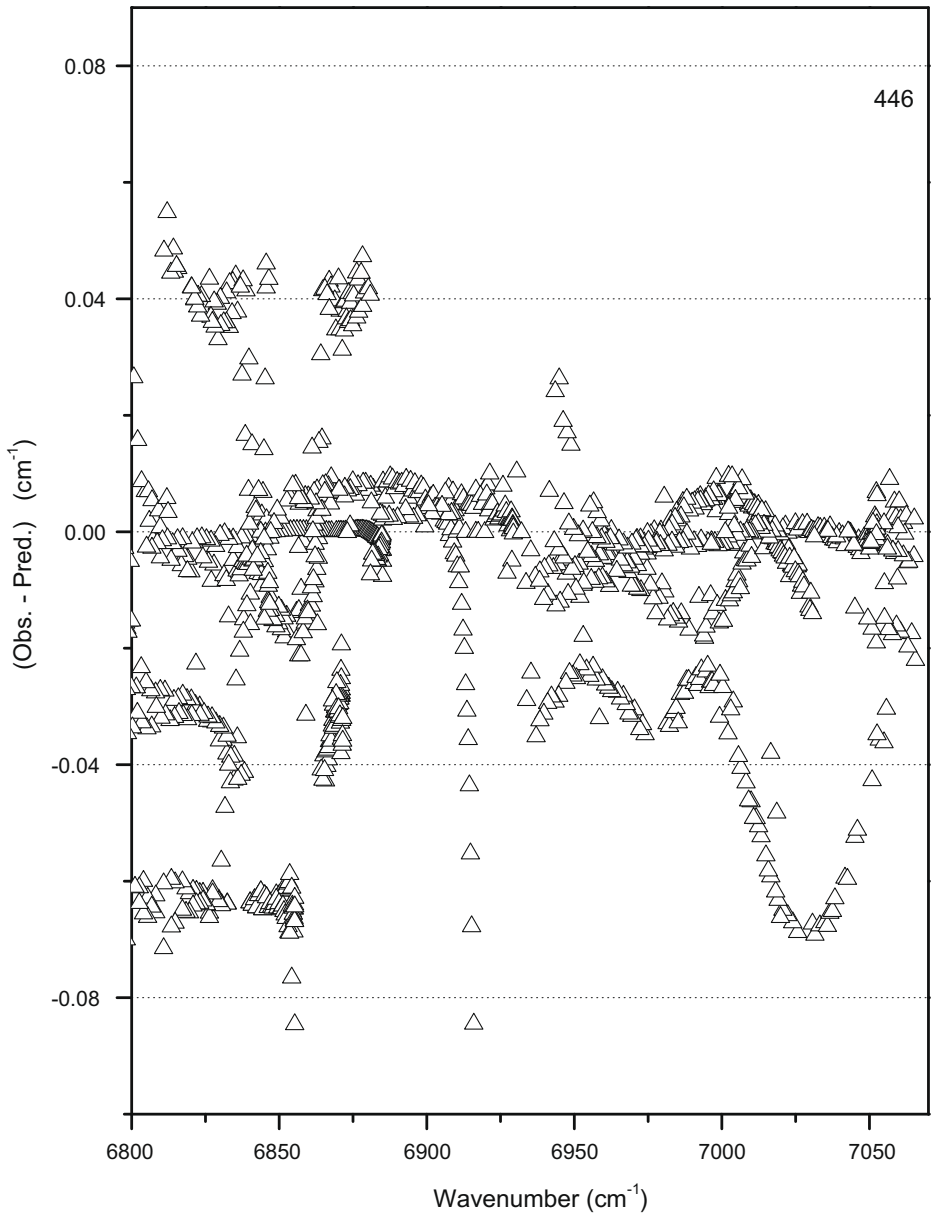

Fig. 5. Difference between the line positions of the $^{14}N_2{}^{16}O$ isotopologue of nitrous oxide assigned in the CW-CRDS spectrum between 6800 and 7066 cm^{-1} and their values predicted by the effective rovibrational Hamiltonian [4].

where absorption lines due to H_2O present as an impurity are superimposed to bands of five N_2O isotopologues including many hot bands, some of them having a lower state energy as high as 2300 cm^{-1} [1,2]. In spite of our careful analysis, about one quarter of the observed transitions has been left unassigned. Most of them are weak lines with line strength values smaller than 5×10^{-26} cm/molecule. We exclude that a high fraction of these unassigned lines is due to unidentified impurities. As the present measurements have evidenced significant deviations between the observations and the predictions of the effective Hamiltonian model, they will help to refine its parameters values which, in turn will help to further decrease the fraction of unassigned transitions.

Acknowledgments

This work was performed in the frame of the European research network QUASAAR (MRTN-CT-2004-512202) and is supported by a collaborative project between CNRS and CAS-China (PICS Grant No. 3359), and between RFBR-Russia and NSFC–China (Grant Nos. 06-05-39016 and 20473079). The support of the Programme National LEFE (CHAT) INSU-CNRS is acknowledged.

Appendix A. Supplementary data

Supplementary data associated with this article can be found, in the online version, at doi:10.1016/j.jms.2008.12.006.

References

[1] A.W. Liu, S. Kassi, P. Malara, D. Romanini, V.I. Perevalov, S.A. Tashkun, S.M. Hu, A. Campargue, J. Mol. Spectrosc. 244 (2007) 33–47.
[2] A.W. Liu, S. Kassi, V.I. Perevalov, S.A. Tashkun, A. Campargue, J. Mol. Spectrosc. 244 (2007) 48–62.
[3] J.-L. Teffo, V.I. Perevalov, O.M. Lyulin, J. Mol. Spectrosc. 168 (1994) 390–403.

[4] V.I. Perevalov, S.A. Tashkun, J.-L. Teffo, Sixteenth Colloquium on High Resolution Molecular Spectroscopy, Dijon (France), 6–10 September 1999, Poster D2, p. 103.
[5] A.V. Vlasova, B.V. Perevalov, S.A. Tashkun, V.I. Perevalov, Fifteenth Symposium on High Resolution Molecular Spectroscopy, Tomsk (Russia), 18–21 July 2006, Poster D20, p. 86.
[6] A. V. Vlasova, B. V. Perevalov, S. A. Tashkun, V. I. Perevalov Proc. SPIE, vol. 6580, 658007 (December 12, 2006).
[7] L.S. Rothman, D. Jacquemart, A. Barbe, D.C. Benner, M. Birk, L.R. Brown, M.R. Carleer, C. Chackerian Jr., K. Chance, L.H. Coudert, V. Dana, V. Malathy Devi, J.-M. Flaud, R.R. Gamache, A. Goldman, J.-M. Hartmann, K.W. Jucks, A.G. Maki, J.-Y. Mandin, S.T. Massie, J. Orphal, A. Perrin, C.P. Rinsland, M.A.H. Smith, J. Tennyson, R.N. Tolchenov, J. Vander Auwera, P. Varanasi, G. Wagner, J. Quant. Spectrosc. Radiat. Transfer 96 (2005) 139–204.
[8] J. Morville, D. Romanini, A.A. Kachanov, M. Chenevier, Appl. Phys. B 78 (2004) 465–476.
[9] Y. Ding, P. Macko, D. Romanini, V. Perevalov, S.A. Tashkun, J.-L. Teffo, S.-M. Hu, A. Campargue, J. Mol. Spectrosc. 226 (2004) 146–160.
[10] M.-R. De Backer-Barilly, Vl.G. Tyuterev, D. Romanini, B. Moeskops, A. Campargue, J. Mol. Struct. 780–781 (2005) 225–233.
[11] A. Campargue, S. Kassi, D. Romanini, A. Barbe, M.-R. De Backer-Barilly, Vl.G. Tyuterev, J. Mol. Spectrosc. 240 (2006) 1–13.
[12] R.A. Toth, J. Mol. Spectrosc. 197 (1999) 158–187.
[13] G. Weirauch, A.A. Kachanov, A. Campargue, M. Bach, J. Vander Auwera, M. Herman, J. Mol. Spectrosc. 202 (2000) 98–106.
[14] L. Wang, V.I. Perevalov, S.A. Tashkun, B. Gao, L.-Y. Hao, S.-M. Hu, J. Mol. Spectrosc. 237 (2006) 129–136.
[15] H.Y. Ni, K.F. Song, V.I. Perevalov, S.A. Tashkun, A.W. Liu, L. Wang, S.M. Hu, J. Mol. Spectrosc. 248 (2007) 55–69.
[16] L. Daumont, J. Vander Auwera, J.-L. Teffo, V.I. Perevalov, S.A. Tashkun, J. Quant. Spectrosc. Radiat. Transfer 104 (2007) 342–356.
[17] H. Oshika, A. Toba, M. Fujitake, N. Ohashi, J. Mol. Spectrosc. 197 (1999) 324–325.